Bulletin of the Earthquake
Research Institute
Vol. 48 (1970), pp. 613-635

33. A Long Wave around a Breakwater with Finite Thickness [I].

— Case of Normal Incidence —

By Takao Momoi,
Earthquake Research Institute.

(Read May 26, 1970.—Received May 30, 1970.)

Abstract

In this paper, the effect of thickness of the breakwater is discussed, where the breakwater runs along a straight line with small aperture and the incident wave invades the breakwater normally. The analysis is based on the buffer domain method. The conspicuous feature disclosed are such that the theory for the breakwater of infinitesimal thickness can be employed for the elucidation of the wave behavior around the prevailing breakwaters of finite thickness in the actual harbours.

1. Introduction

Succeeding the previous works (*Momoi*, 1967a—1969c) entitled "A Long Wave around a Breakwater" in which the breakwater has infinitesimal thickness, the long wave around the breakwater with finite thickness will be discussed in the present and subsequent papers under the title "A Long Wave around a Breakwater with Finite Thickness". To begin with, the case of the normal incidence of the invading wave is treated in this paper.

2. Rigorous Theory

2,1. Model Used and Nomenclature.

The breakwater is assumed to be a plate of finite thickness l (refer to Fig. 1), which is located in the waters of uniform depth H along the straight line with gap of breadth $2d$. The x-axis runs along the wall facing the windward waters, the y-axis being taken normally through the midpoint of the gap. A train of periodic waves is then propagated normally against the breakwater, which is stated by

$$\exp(-i\omega t - iky), \tag{1}$$

where

ω: the angular frequency of the incident wave,

k: the wave number of the incident wave,

t: the time variable.

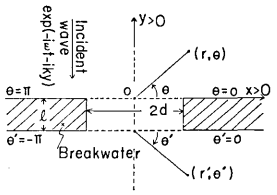

Fig. 1. Model used and the nomenclature.

2,2. Equation and Boundary Conditions.

The equation employed is the long wave equation, i.e.,

$$\frac{1}{c^2}\frac{\partial^2\zeta'}{\partial t^2}=\frac{\partial^2\zeta'}{\partial x^2}+\frac{\partial^2\zeta'}{\partial y^2} \tag{2}$$

where

ζ': the elevation of water surface,

c : the velocity of long wave.

For the case of periodic waves, equation (2) is reduced to

$$\frac{\partial^2\zeta}{\partial x^2}+\frac{\partial^2\zeta}{\partial y^2}+k^2\zeta=0, \tag{3}$$

where $\zeta'=\zeta\exp(-i\omega t)$.

Using the polar coordinate $(r,\ \theta)$, equation (3) is written as follows.

$$\frac{\partial^2\zeta}{\partial r^2}+\frac{1}{r}\frac{\partial\zeta}{\partial r}+\frac{1}{r^2}\frac{\partial^2\zeta}{\partial\theta^2}+k^2\zeta=0. \tag{4}$$

As for the boundary conditions at the rigid wall, we have

$$\frac{\partial\zeta}{\partial y}=0 \quad (y=0 \text{ and } -l \text{ for } |x|>d) \tag{5}$$

and

$$\frac{\partial\zeta}{\partial x}=0 \quad (|x|=d \text{ for } y=0 \text{ to } -l). \tag{6}$$

2,3. Formal Solutions.

In this section, the formal solutions of the wave are presented. The principle of the analysis is the method of the buffer domain introduced firstly by the author. The outline of this method is described in Section *2,3* of the first paper concerning the long wave around the breakwater (*Momoi*, 1967a).

Referring to Fig. 2, all the domains are separated into five parts, i. e.,

the domain $D_1: 0<\theta<\pi$ and $r>d$,
the domain $B_1: 0<\theta<\pi$ and $r<d$,
the domain $D_2: |x|<d$ and $0>y>-l$,
the domain $B_2: r'<d$ and $0>\theta'>-\pi$,
the domain $D_3: r'>d$ and $0>\theta'>-\pi$.

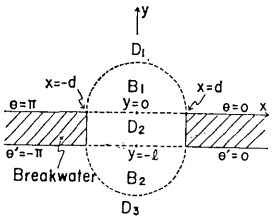

Fig. 2. Illustration of the domains defined.

For the nomenclature of (r', θ'), Fig. 1 should be referred to. The domains defined in the above are illustrated in Fig. 2. Among these domains, $D_j(j=1, 2, 3)$ are the non-buffer domains and $B_j(j=1, 2)$ the buffer domains in our method.

Let $\zeta_j(j=1, B1, 2, B2, 3)$ be the wave heights in the domains D_1, B_1, D_2, B_2 and D_3 with the abbreviation of the time factor $\exp(-i\omega t)$. The formal solutions are then expressed as

$$\zeta_1=2\cos ky+\sum_{m=0}^{\infty}\zeta_1^{(2m)}H_{2m}^{(1)}(kr)\cos 2m\theta \tag{7}$$

in domain D_1,

$$\zeta_{B1}=\sum_{m=0}^{\infty}\{\bar{\zeta}_{B1}^{(2m)}J_{2m}(kr)\cos 2m\theta+\zeta_{B1}^{(2m+1)}J_{2m+1}(kr)\sin(2m+1)\theta\} \tag{8}$$

in domain B_1,

$$\zeta_2=\sum_{m=0}^{\infty}\{\bar{\zeta}_2^{(m)}\exp(-ik_m y)+\zeta_2^{(m)}\exp(+ik_m y)\}\cos\frac{m\pi}{d}x \tag{9}$$

in domain D_2,

$$\zeta_{B2}=\sum_{m=0}^{\infty}\{\bar{\zeta}_{B2}^{(2m)}J_{2m}(kr')\cos 2m\theta'+\zeta_{B2}^{(2m+1)}J_{2m+1}(kr')\sin(2m+1)\theta'\} \tag{10}$$

in domain B_2

and

$$\zeta_3=\sum_{m=0}^{\infty}\zeta_3^{(2m)}H_{2m}^{(1)}(kr')\cos 2m\theta' \tag{11}$$

in domain D_3,

where $\zeta_1^{(2m)}$, $\bar{\zeta}_{B1}^{(2m)}$, $\zeta_{B1}^{(2m+1)}$, $\bar{\zeta}_2^{(m)}$, $\zeta_2^{(m)}$, $\bar{\zeta}_{B2}^{(2m)}$, $\zeta_{B2}^{(2m+1)}$ and $\zeta_3^{(2m)}$ are the unknown factors to be determined by the conditions between the adjacent domains and

$$k_m=\sqrt{k^2-\left(\frac{m\pi}{d}\right)^2}. \tag{12}$$

2,4. Infinite Simultaneous Equations.

The infinite simultaneous equations are derived from the formal solutions obtained in the foregoing section and the conditions between

the neighbouring domains, i. e.,

$$\left.\begin{aligned}\zeta_1&=\zeta_{B1}\\ \frac{\partial\zeta_1}{\partial r}&=\frac{\partial\zeta_{B1}}{\partial r}\end{aligned}\right\}\quad\text{at}\quad r=d\quad\text{and}\quad 0<\theta<\pi,\tag{13}$$

$$\left.\begin{aligned}\zeta_{B1}&=\zeta_2\\ \frac{\partial\zeta_{B1}}{\partial y}&=\frac{\partial\zeta_2}{\partial y}\end{aligned}\right\}\quad\text{at}\quad y=0\quad\text{and}\quad |x|<d,\tag{14}$$

$$\left.\begin{aligned}\zeta_2&=\zeta_{B2}\\ \frac{\partial\zeta_2}{\partial y}&=\frac{\partial\zeta_{B2}}{\zeta y}\end{aligned}\right\}\quad\text{at}\quad y=-l\quad\text{and}\quad |x|<d,\tag{15}$$

and

$$\left.\begin{aligned}\zeta_{B2}&=\zeta_3\\ \frac{\partial\zeta_{B2}}{\partial r}&=\frac{\partial\zeta_3}{\partial r}\end{aligned}\right\}\quad\text{at}\quad r'=d\quad\text{and}\quad 0>\theta'>-\pi.\tag{16}$$

Substituting (7) and (8) into (13), and applying the operator

$$\int_0^\pi \cos 2m\theta\, d\theta\quad(m=0, 1, 2, \cdots)$$

to (13), we have

$$\begin{aligned}&\begin{Bmatrix}J_{2m}\\ J'_{2m}\end{Bmatrix}\bar{\zeta}_{B1}^{(2m)}+\frac{1}{\varepsilon_m}\frac{2}{\pi}\sum_{n=0}^{\infty}\frac{2n+1}{(2n+1)^2-(2m)^2}\begin{Bmatrix}J_{2n+1}\\ J'_{2n+1}\end{Bmatrix}\zeta_{B1}^{(2n+1)}\\ &=\begin{Bmatrix}H_{2m}^{(1)}\\ H_{2m}^{(1)\prime}\end{Bmatrix}\zeta_1^{(2m)}+\frac{2}{\varepsilon_m}\begin{Bmatrix}J_{2m}\\ J'_{2m}\end{Bmatrix}\qquad(m=0, 1, 2, \cdots).\end{aligned}\tag{17}$$

In the above,
$$\left.\begin{aligned}\varepsilon_m&=1\quad(m=0)\\ &=1/2\quad(m>0),\end{aligned}\right\}$$

and J_p, J'_p, $H_p^{(1)}$ and $H_p^{(1)\prime}$ are the abbreviations of $J_p(kd)$, $J'_p(kd)$, $H_p^{(1)}(kd)$ and $H_p^{(1)\prime}(kd)$ (p : non-negative integers). The expressions in the wavy bracket are taken in the same order. These conventions are followed in the subsequent reductions, unless otherwise stated.

Likewise, substituting (8)—(10) into (14) and (15), and applying the operator

$$\int_{-d}^{d}\cos\frac{m\pi}{d}x\,dx\qquad(m=0, 1, 2, \cdots)$$

to them, we have

$$\left.\begin{aligned}\sum_{n=0}^{\infty} K_{n,m}\bar{\zeta}_{B1}^{(2n)} &= \varepsilon_m kd(\bar{\zeta}_2^{(m)}+\zeta_2^{(m)})\\ \sum_{n=0}^{\infty} L_{n,m}\zeta_{B1}^{(2n+1)} &= -i\varepsilon_m k_m d(\bar{\zeta}_2^{(m)}-\zeta_2^{(m)})\end{aligned}\right\}, \tag{18}$$

$$\left.\begin{aligned}\sum_{n=0}^{\infty} K_{n,m}\bar{\zeta}_{B2}^{(2n)} &= \varepsilon_m kd\{\bar{\zeta}_2^{(m)}\exp(+ik_m l)+\zeta_2^{(m)}\exp(-ik_m l)\}\\ \sum_{n=0}^{\infty} L_{n,m}\zeta_{B2}^{(2n+1)} &= -i\varepsilon_m k_m d\{\bar{\zeta}_2^{(m)}\exp(+ik_m l)-\zeta_2^{(m)}\exp(-ik_m l)\}\end{aligned}\right\}, \tag{19}$$

where

$$\left.\begin{aligned}K_{n,m} &= \int_0^{kd} J_{2n}(z)\cos\frac{m\pi}{kd}z\,dz\\ L_{n,m} &= (2n+1)\int_0^{kd}\frac{J_{2n+1}(z)}{z}\cos\frac{m\pi}{kd}z\,dz\end{aligned}\right\} \tag{20}$$

and $m=0, 1, 2, \cdots$.

The substitution of (10) and (11) into (16) and the application of the operator

$$\int_{-\pi}^{0}\cos 2m\theta' d\theta' \qquad (m=0, 1, 2, \cdots)$$

to (16) yield

$$\begin{aligned}&\begin{Bmatrix}J_{2m}\\ J'_{2m}\end{Bmatrix}\bar{\zeta}_{B2}^{(2m)}-\frac{1}{\varepsilon_m}\frac{2}{\pi}\sum_{n=0}^{\infty}\frac{2n+1}{(2n+1)^2-(2m)^2}\begin{Bmatrix}J_{2n+1}\\ J'_{2n+1}\end{Bmatrix}\zeta_{B2}^{(2n+1)}\\ &=\begin{Bmatrix}H_{2m}^{(1)}\\ H_{2m}^{(1)\prime}\end{Bmatrix}\zeta_3^{(2m)} \qquad (m=0, 1, 2, \cdots).\end{aligned} \tag{21}$$

Eliminating, respectively, $\zeta_1^{(2m)}$ from (17) and $\zeta_3^{(2m)}$ from (21), these are reduced to

$$\begin{aligned}&\frac{i}{kd}\begin{Bmatrix}\bar{\zeta}_{B1}^{(2m)}\\ \bar{\zeta}_{B2}^{(2m)}\end{Bmatrix}\pm\frac{1}{\varepsilon_m}\sum_{n=0}^{\infty}\frac{2n+1}{(2n+1)^2-(2m)^2}(J_{2n+1}H_{2m}^{(1)\prime}-J'_{2n+1}H_{2m}^{(1)})\begin{Bmatrix}\zeta_{B1}^{(2n+1)}\\ \zeta_{B2}^{(2n+1)}\end{Bmatrix}\\ &=\begin{Bmatrix}\dfrac{2}{\varepsilon_m} & \dfrac{i}{kd}\\ 0\end{Bmatrix} \qquad (m=0, 1, 2, \cdots),\end{aligned} \tag{22}$$

where the double sign $\pm$ is taken in the same order as the expressions in the wavy bracket. This convention is followed in the later reductions.

Solving (18) and (19) with respect to $\bar{\zeta}_2^{(m)}$ and $\zeta_2^{(m)}$, we have

$$\begin{Bmatrix}\bar{\zeta}_2^{(m)}\\ \zeta_2^{(m)}\end{Bmatrix}=\frac{1}{2\varepsilon_m kd}\sum_{n=0}^{\infty}K_{n,m}\bar{\zeta}_{B1}^{(2n)}\pm\frac{i}{2\varepsilon_m k_m d}\sum_{n=0}^{\infty}L_{n,m}\zeta_{B1}^{(2n+1)} \tag{23}$$

and

$$\begin{Bmatrix}\bar{\zeta}_2^{(m)}\\ \zeta_2^{(m)}\end{Bmatrix}\exp(\pm ik_m l)=\frac{1}{2\varepsilon_m kd}\sum_{n=0}^{\infty}K_{n,m}\bar{\zeta}_{B2}^{(2n)}\pm\frac{i}{2\varepsilon_m k_m d}\sum_{n=0}^{\infty}L_{n,m}\zeta_{B2}^{(2n+1)},\qquad(24)$$

where $m=0, 1, 2, \cdots$. These equations are used in the calculations of $\bar{\zeta}_2^{(m)}$ and $\zeta_2^{(m)}$.

Using (23) and (24), the equations with respect to only $\bar{\zeta}_{B1}^{(2n)}$, $\zeta_{B1}^{(2n+1)}$, $\bar{\zeta}_{B2}^{(2n)}$ and $\zeta_{B2}^{(2n+1)}$ are arrived at. These are described as

$$k_m d\begin{Bmatrix}\cos k_m l\\ \sin k_m l\end{Bmatrix}\sum_{n=0}^{\infty}K_{n,m}\bar{\zeta}_{B1}^{(2n)}\mp kd\begin{Bmatrix}\sin k_m l\\ \cos k_m l\end{Bmatrix}\sum_{n=0}^{\infty}L_{n,m}\zeta_{B1}^{(2n+1)}$$
$$-\begin{Bmatrix}k_m d\\ kd\end{Bmatrix}\sum_{n=0}^{\infty}\begin{Bmatrix}K_{n,m}\bar{\zeta}_{B2}^{(2n)}\\ L_{n,m}\zeta_{B2}^{(2n+1)}\end{Bmatrix}=0,\qquad(25)$$

where $m=0, 1, 2, \cdots$.

Equations (22) and (25) are now the infinite simultaneous equations to be obtained.

2,5. Reduction to Finite Simultaneous Equations.

In this section, the infinite simultaneous equations are reduced to the finite simultaneous equations being accessible to the calculations by the electronic computer.

The approximation

$$\left.\begin{aligned}J_m(z)&\neq 0\quad(m\leqq 2p+1)\\ J_m(z)&\equiv 0\quad(m>2p+1)\end{aligned}\right\}\qquad(p:\text{positive integers})\qquad(26)$$

for $z\leqq kd$ is applied upon expressions (8) and (10) in the buffer domains B_1 and B_2.

Using approximation (26), equations (22) and (25) are reduced to

$$\frac{i}{kd\,J_{2m}H_{2m}^{(1)\prime}}\begin{Bmatrix}X_{2m+1}\\ X_{2m+1+2(p+1)}\end{Bmatrix}$$
$$\pm\frac{1}{\varepsilon_m}\sum_{n=0}^{p}\frac{2n+1}{(2n+1)^2-(2m)^2}\left(1-\frac{J'_{2n+1}H_{2m}^{(1)}}{J_{2n+1}H_{2m}^{(1)\prime}}\right)\begin{Bmatrix}X_{2n+2}\\ X_{2n+2+2(p+1)}\end{Bmatrix}$$
$$=\begin{Bmatrix}\dfrac{2i}{\varepsilon_m kd\,H_{2m}^{(1)\prime}}\\ 0\end{Bmatrix}\qquad(m=0, 1, 2, \cdots, p)\qquad(27)$$

and

$$k_m d\exp(+ik_m l)\begin{Bmatrix}\cos k_m l\\ \sin k_m l\end{Bmatrix}\sum_{n=0}^{p}\frac{K_{n,m}}{J_{2n}}X_{2n+1}$$
$$\mp kd\exp(+ik_m l)\begin{Bmatrix}\sin k_m l\\ \cos k_m l\end{Bmatrix}\sum_{n=0}^{p}\frac{L_{n,m}}{J_{2n+1}}X_{2n+2}$$

$$-\begin{Bmatrix} k_m d \\ kd \end{Bmatrix} \exp(+ik_m l) \sum_{n=0}^{p} \begin{Bmatrix} \dfrac{K_{n,m}}{J_{2n}} X_{2n+1+2(p+1)} \\ \dfrac{L_{n,m}}{J_{2n+1}} X_{2n+2+2(p+1)} \end{Bmatrix} = 0 \quad (m=0, 1, 2, \cdots, p), \tag{28}$$

where

$$\left.\begin{aligned} X_{2m+1} &= \bar{\zeta}_{B1}^{(2m)} J_{2m}, \\ X_{2m+2} &= \zeta_{B1}^{(2m+1)} J_{2m+1}, \\ X_{2m+1+2(p+1)} &= \bar{\zeta}_{B2}^{(2m)} J_{2m}, \\ \text{and} \quad X_{2m+2+2(p+1)} &= \zeta_{B2}^{(2m+1)} J_{2m+1}. \end{aligned}\right\} \tag{29}$$

Equations (27) and (28) are normalized in order to avoid the truncation errors in the numerical calculation by the computer. The normalization factors are $J_{2n+1} H_{2m}^{(1)\prime}$ in (27) and $\exp(+ik_m l)$ in (28).

Using $4(p+1)$ equations (27) and (28), the unknowns $X_n (n=1$ to $4p+4)$ are calculated through the use of the electronic computer.

2,6. Flow of Numerical Calculation.

The unknown factors

$$\bar{\zeta}_{B1}^{(2m)},\ \zeta_{B1}^{(2m+1)},\ \bar{\zeta}_{B2}^{(2m)} \quad \text{and} \quad \zeta_{B2}^{(2m+1)} \qquad (m=0, 1, 2, \cdots, p) \tag{30}$$

in the domains $B_j (j=1, 2)$ are calculated by simultaneous equations (27) and (28) through expressions (29).*

The substitution of (30) into the first of (23) and the second of (24) yields

$$\bar{\zeta}_2^{(m)} \quad \text{and} \quad \zeta_2^{(m)} \exp(-ik_m l) \qquad (m=0, 1, 2, \cdots), \tag{31}$$

where the upper limit of $\sum$ in (23) and (24) is set equal to p. Allowing for the errors due to the truncation, the unknown $\zeta_2^{(m)}$ with factor $\exp(-ik_m l)$ is calculated instead of only $\zeta_2^{(m)}$.

As for the unknown factors in the domains $D_j (j=1, 3)$, the substitution of (30) into the first of (17) and (21) gives

$$\zeta_1^{(2m)} \quad \text{and} \quad \zeta_3^{(2m)} \qquad (m=0, 1, 2, \cdots). \tag{32}$$

In using (17) and (21), approximation (26) and its result, i. e.,

$$\bar{\zeta}_j^{(2m)} \equiv \zeta_j^{(2m+1)} \equiv 0 \qquad (j=B1, B2)$$

for $m>p$ are employed.

* In the calculation of (27) and (28), integrals $K_{n,m}$ and $L_{n,m}$ are computed by the same procedure as that described in Section 2 of the fifth paper concerning the long wave around an estuary (*Momoi*, 1968d).

The wave behavior around the breakwater is now investigated by formal expressions (7) to (11) through the substitution of (30) to (32). In the calculations of (8), (9) and (10), the upper limits of (8) and (10) are taken as p in accordance with the approximation employed and the second term of (9) is transformed into a form excluding the accumulation of the truncation error, i. e.,

$$\zeta_2^{(m)} \exp(+ik_m y) = \{\zeta_2^{(m)} \exp(-ik_m l)\} \exp\{+ik_m(y+l)\} \qquad (y=0 \text{ to } -l).$$

The numerical calculations and the discussions of their results will be given in the later section.

3. Approximated Theory for Very Long Wave

3,1. Model Used and Nomenclature.

The model used and the coordinate system are the same as those employed in Section 2 (case of the rigorous theory). In the present case, the incident wave is described as

$$\exp(+i\omega t+iky) \tag{33}$$

in place of $\exp(-i\omega t-iky)$, where the notation is the same as that in Section 2.

3,2. Equation and Boundary Conditions.

The governing equation is given by (3) with replacement $\exp(-i\omega t)$ to $\exp(+i\omega t)$. The boundary conditions are expressed by (5) and (6).

3,3. Solutions.

In this section, the solution is given under the restriction $2d \ll L$, where L is the wave-length and $2d$ the width of the breakwater gap as shown in Fig. 3.

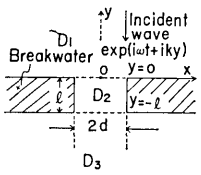

Fig. 3. Illustration of the domains defined in the case $d \ll L$, where L is the wave-length.

Referring to Fig. 3, the entire domain is separated into three parts, i. e.,

the domain $D_1 : y>0$,
the domain $D_2 : |x|<d$ and $0>y>-l$,
the domain $D_3 : y<-l$.

Let $F_j(x, y)$ $(j=1, 2, 3)$ be the wave heights in the domains D_j $(j=1, 2, 3)$ with the abbreviation of the time factor $\exp(+i\omega t)$. The formal solutions are expressed as

$$F_1(x, y)=2\cos ky+\chi_1(x, y) \tag{34}$$

in domain D_1,

$$F_2(x, y)=A_p\exp(+iky)+A_r\exp(-iky) \tag{35}$$

in domain D_2,

and

$$F_3(x, y)=\chi_3(x, y) \tag{36}$$

in domain D_3,

where χ_j $(j=1, 3)$ are the waves scattered by the breakwater gap, and A_j $(j=p, r)$ the amplitudes of the progressive and retrogressive waves in the gap. Expression (35) in the gap has no higher modes reflecting the limitation $2d\ll L$. This assumption is considered to be acceptable from the physical point of view. The above procedure goes along the same lines as that devised by Ippen and Goda (1963) or Mitsui (1966). Following their procedure, the development of the theory is carried out.

Substituting expression (34) into (3) and applying the Fourier transform

$$X_1(\beta, y)=\frac{1}{\sqrt{2\pi}}\int_{-\infty}^{\infty}\chi_1(x, y)e^{-i\beta x}dx \tag{37}$$

to it, we have

$$\frac{d^2X_1}{dy^2}-\gamma^2X_1=0,$$

where

$$\gamma=\sqrt{\beta^2-k^2}.$$

Solving the above equation with allowance for $\chi_1\to 0$ $(y\to\infty)$, the solution becomes

$$X_1=C_1\exp(-\gamma y), \tag{38}$$

where C_1 is unknown factor.

Using the inverse Fourier transform of (37) and (38), (34) is expressed as

$$F_1(x, y)=2\cos ky+\frac{1}{\sqrt{2\pi}}\int_{-\infty}^{\infty}C_1\exp(-\gamma y)e^{i\beta x}d\beta. \tag{39}$$

Likewise, expression (36) becomes

$$F_3(x, y)=\frac{1}{\sqrt{2\pi}}\int_{-\infty}^{\infty}C_3\exp(\gamma y)e^{i\beta x}d\beta. \tag{40}$$

Using the condition that the velocity of the y-component at $y=0$ and $-l$ must be continuous, i. e.,

$$\frac{\partial F_2}{\partial y}=\begin{cases}\dfrac{\partial F_1}{\partial y} & \text{at} \quad y=0\\ \dfrac{\partial F_3}{\partial y} & \text{at} \quad y=-l\end{cases}$$

and expressions (35), (39) and (40), we have

$$\left.\begin{aligned} C_1&=-i\sqrt{\frac{2}{\pi}}(A_p-A_r)\frac{kd\sin\beta d}{\beta d\,\gamma},\\ C_3&=i\sqrt{\frac{2}{\pi}}\left\{A_p\exp(-ikl)-A_r\exp(+ikl)\right\}\frac{kd\sin\beta d}{\beta d\,\gamma}\exp(\gamma l).\end{aligned}\right\} \tag{41}$$

Substituting (41) into (39) and (40), these are reduced to

$$\left.\begin{aligned} F_1(x,y)&=2\cos ky-\frac{2i}{\pi}(A_p-A_r)f(x,y),\\ F_3(x,y)&=\frac{2i}{\pi}\left\{A_p\exp(-ikl)-A_r\exp(+ikl)\right\}f(x,-l-y),\end{aligned}\right\} \tag{42}$$

where

$$f(x,z)=kd\int_0^\infty\frac{\sin\xi\exp(-\sqrt{\xi^2-(kd)^2}\cdot z/d)}{\xi\sqrt{\xi^2-(kd)^2}}\cos(\xi x/d)d\xi. \tag{43}$$

In order to determine A_p and A_r, the mean levels of water at $y=0$ and $-l$ are equated. These are expressed as

$$\left.\begin{aligned} \frac{1}{2d}\int_{-d}^{d}F_1(x,0)dx&=\frac{1}{2d}\int_{-d}^{d}F_2(x,0)dx,\\ \frac{1}{2d}\int_{-d}^{d}F_2(x,-l)dx&=\frac{1}{2d}\int_{-d}^{d}F_3(x,-l)dx.\end{aligned}\right\} \tag{44}$$

Substituting (35) and (42) into (44), we have

$$\left.\begin{aligned} A_p&=\frac{1}{iB}\exp(ikl)\left(1+\frac{2iI}{\pi}\right)\\ \text{and}\qquad A_r&=\frac{-1}{iB}\exp(-ikl)\left(1-\frac{2iI}{\pi}\right),\end{aligned}\right\} \tag{45}$$

where

$$\left.\begin{aligned} I&=kd\int_0^\infty\frac{\sin^2\xi}{\xi^2\sqrt{\xi^2-(kd)^2}}d\xi\\ \text{and}\qquad B&=\left\{1-\left(\frac{2I}{\pi}\right)^2\right\}\sin kl+\frac{4I}{\pi}\cos kl.\end{aligned}\right\} \tag{46}$$

Using (45), expressions (35) and (42) become as follows.

$$F_1(x, y)=2\cos ky-\frac{4}{\pi B}\left(\cos kl-\frac{2I}{\pi}\sin kl\right)f(x, y), \tag{47}$$

$$F_2(x, y)=\frac{1}{B}\left\{2\sin k(l+y)+\frac{4I}{\pi}\cos k(l+y)\right\} \tag{48}$$

and

$$F_3(x, y)=\frac{4}{\pi B}f(x, -l-y), \tag{49}$$

where I, B and $f(x, z)$ are described in (43) and (46).

Expressions (47) to (49) are the final forms to be obtained for the wave of very long wave-length. The numerical calculations and discussions are made in the later section.

4. Calculations and Discussions

Numerical calculations and the discussions are made in this section.

4,1. Verification of Rigorous Theory.

The validity of the rigorous theory developed in Section 2 is verified by use of approximated theory and the theory for limiting case.

Verification is, to begin with, made by the theory for very long wave which is developed in Section 3. The calculations are carried out for the amplitude along the directions illustrated in Fig. 4 with specifications of $kd=0.1$ and $l/d=1.0$. The results are given in Figs. 5 to 9. According to these figures, the rigorous and approximated theories are in very good agreement for very long wave of the order of $kd\sim 0.1$.

When $l\ll d$, the rigorous theory for the breakwater with finite thickness approaches that with infinitesimal thickness. Setting down $l/d=0.1$, the agreement is put to the test. The results are presented in Figs. 10a, b, c for the amplitude of RST (resultant) wave in the windward and in Figs. 11a, b, c for that in the leeward. The cited values of kd are 0.1, 1.0 and 2.0. The solid lines are the result of the theory of finite thickness in the present work, while the broken lines that of infinitesimal thickness in the previous paper (*Momoi*, 1967a). These figures show that the theory for the breakwater of finite thickness, when the thickness is small, is in good agreement with the theory of infinitesimal thickness.

4,2. RST Wave.

In this section, RST (resultant) wave is discussed. RST wave is calculated by the procedure described in Section 2,6. The computed

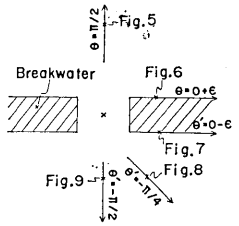

Fig. 4.

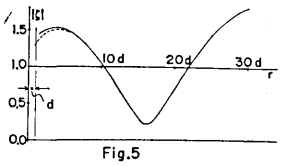

Fig.5

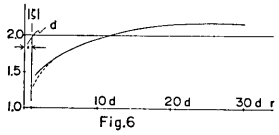

Fig.6

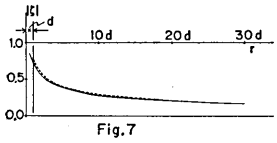

Fig.7

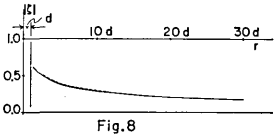

Fig.8

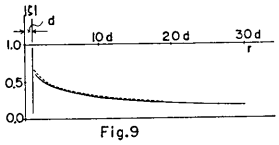

Fig.9

Fig. 4. Directions computed in Figs. 5 to 9.

Figs. 5 to 9. Amplitude variation in typical directions shown in Fig. 4 with specifications of $kd=1.0$ and $l/d=1.0$. The solid and broken lines denote, respectively, the results calculated on the basis of the rigorous and approximated theories.

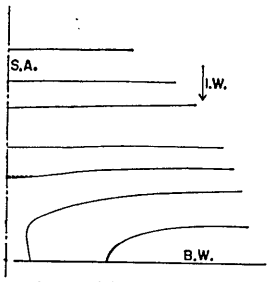

Fig.10a. kd=0.1

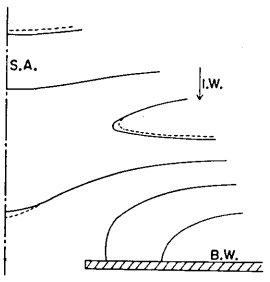

Fig.10b. kd=1.0

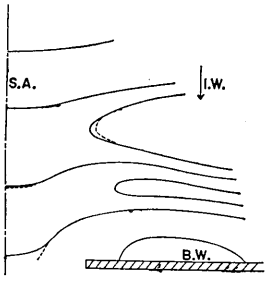

Fig.10c. kd=2.0

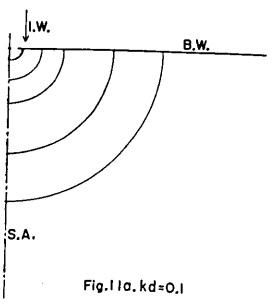

Fig.11a. kd=0.1

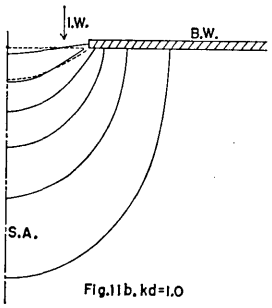

Fig.11b. kd=1.0

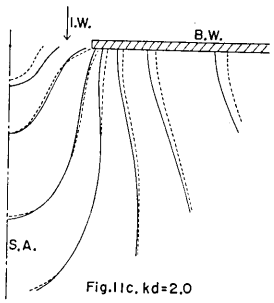

Fig.11c. kd=2.0

Figs. 10a, b, c and 11a, b, c. Comparison of the amplitudes for the case of the breakwater with finite thickness ($l/d=0.1$) and for that with infinitesimal thickness*, the former of which is depicted by the solid line and the latter by the broken line. The first three figures are relevant to the windward and the last three to the leeward.

* **I.W.**, **B.W.** and **S.A.** are respectively the abbreviations of "incident wave", "breakwater" and "symmetric axis". **L** denotes the thickness ratio l/d of the breakwater.

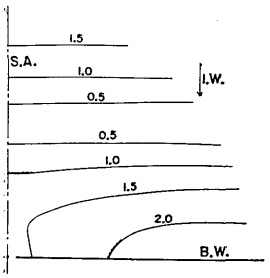

Fig.12-1. kd=0.1, L=0.1

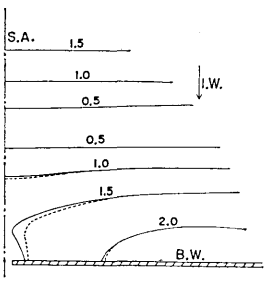

Fig.12-2. kd=0.1, L=0.5

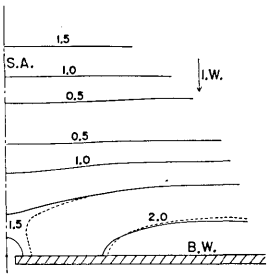

Fig.12-3. kd=0.1, L=1.0

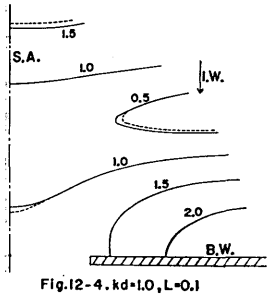

Fig.12-4. kd=1.0, L=0.1

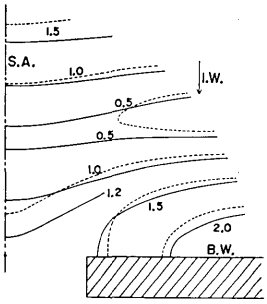

Fig.12-5. kd=1.0, L=0.5

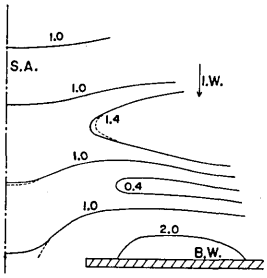

Fig.12-6. kd=2.0, L=0.1

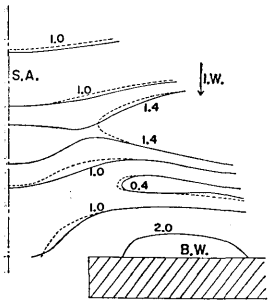

Fig.12-7. kd=2.0, L=0.5

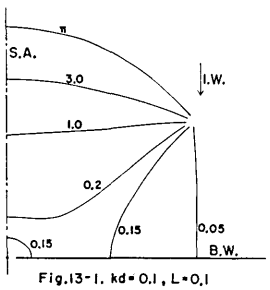

Fig.13-1. kd=0.1, L=0.1

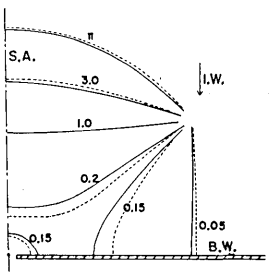

Fig.13-2. kd=0.1, L=0.5

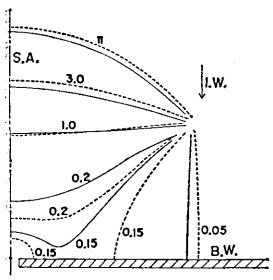

Fig.13-3. kd=0.1, L=1.0

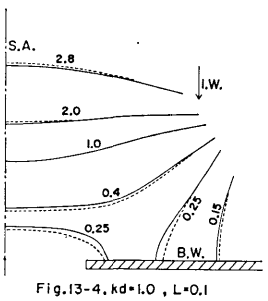

Fig.13-4. kd=1.0, L=0.1

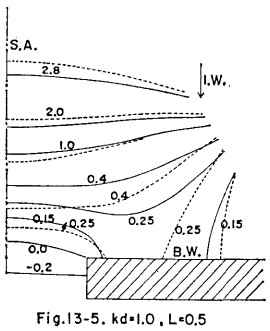

Fig.13-5. kd=1.0, L=0.5

Figs. 12-1 to 12-7. Variation of the amplitude $|\zeta|$ in the windward waters*.
Figs. 13-1 to 13-5. Variation of the phase $\arg\zeta$ in the windward waters*.

* See the footnote of Figs. 10a, b, c and 11a, b. c.

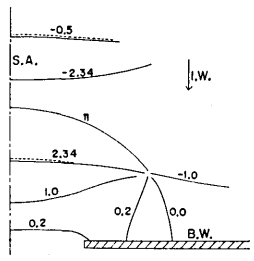

Fig.13-6, kd=2.0, L=0.1

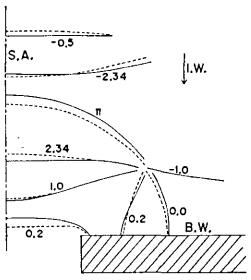

Fig.13-7, kd=2.0, L=0.5

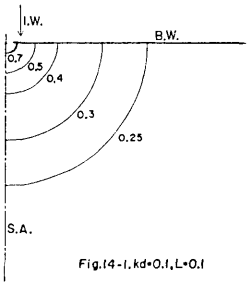

Fig.14-1, kd=0.1, L=0.1

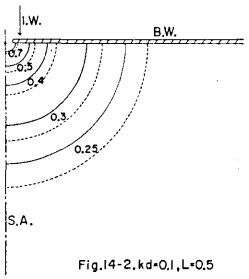

Fig.14-2, kd=0.1, L=0.5

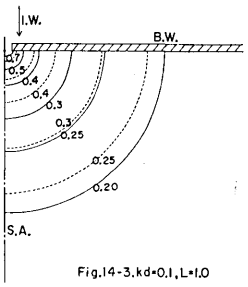

Fig.14-3, kd=0.1, L=1.0

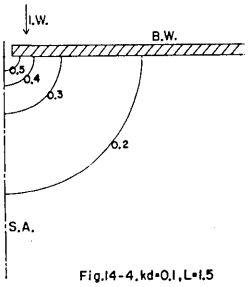

Fig.14-4, kd=0.1, L=1.5

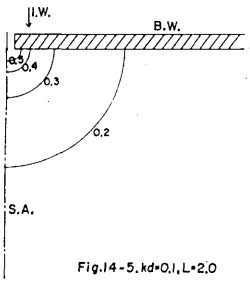

Fig.14-5, kd=0.1, L=2.0

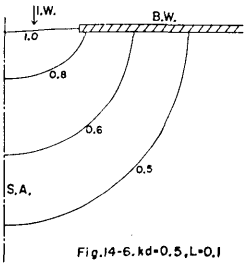

Fig.14-6, kd=0.5, L=0.1

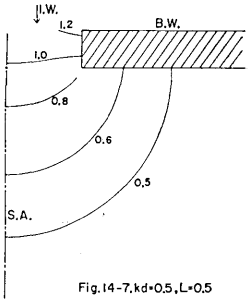

Fig.14-7, kd=0.5, L=0.5

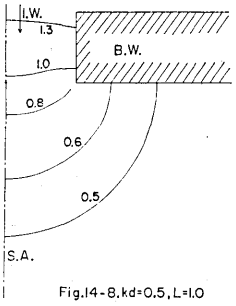

Fig.14-8, kd=0.5, L=1.0

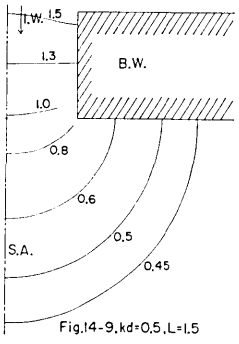

Fig.14-9, kd=0.5, L=1.5

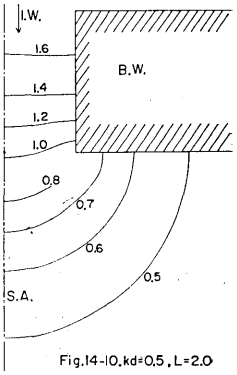

Fig.14-10, kd=0.5, L=2.0

Figs. 13-6 and 13-7. Variation of the phase arg ζ in the windward waters*.
Figs. 14-1 to 14-10. Variation of the amplitude $|\zeta|$ in the leeward waters*.

* See the footnote of Figs. 10a, b, c and 11a, b, c.

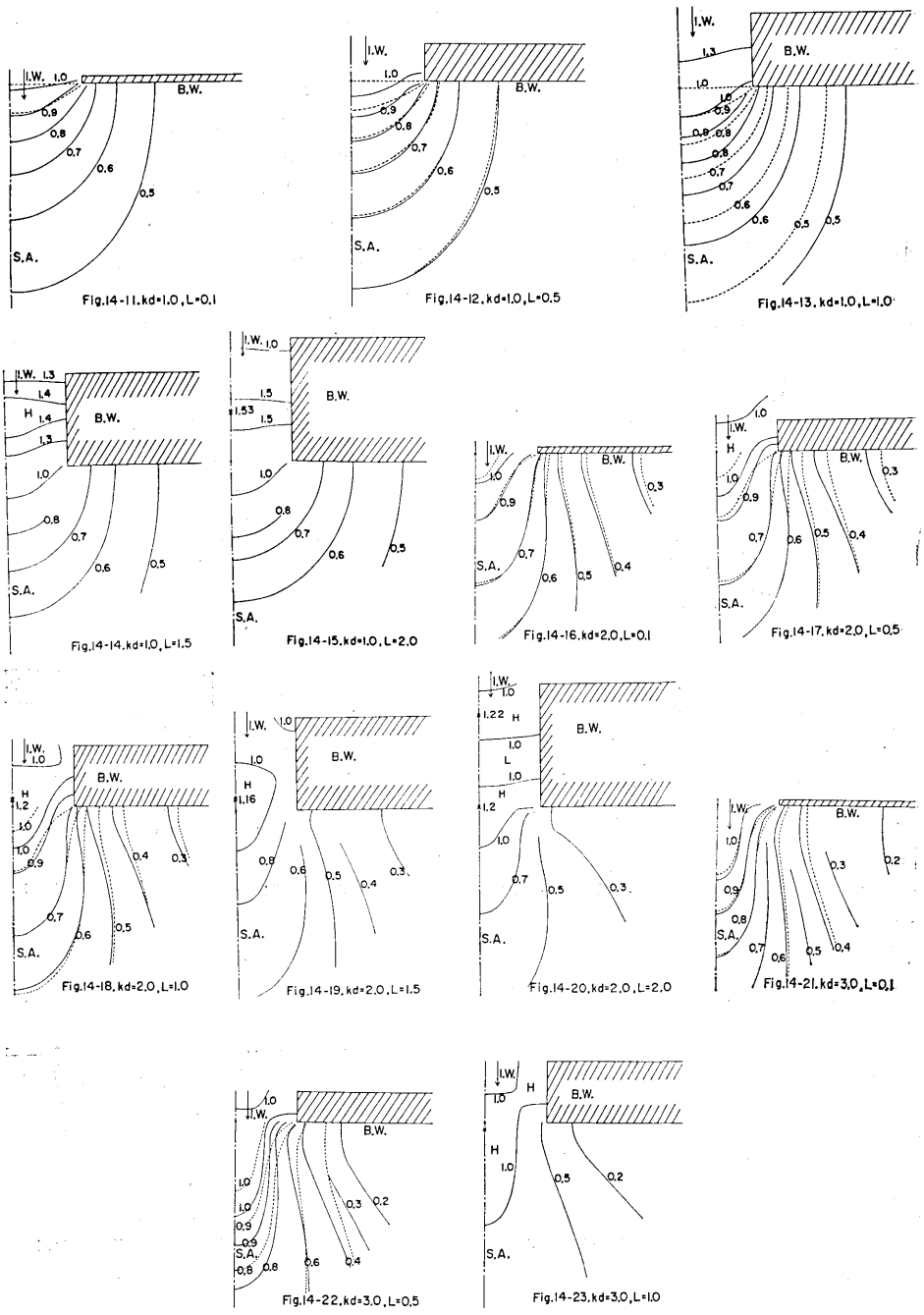

Figs. 14-11 to 14-23. Variation of the amplitude $|\zeta|$ in the leeward waters*.

* See the footnote of Figs. 10a, b, c and 11a, b, c.

range is 0.1 to 3.0 for kd and 0.1 to 2.0 for l/d. The results are presented in Figs. 12-1 (2, 3, ···) to 15-1 (2, 3, ···).* In these figures, the curves based on the theory for *finite* thickness in Section 2 are depicted by the solid lines and those on the basis of the theory for *infinitesimal* thickness in the previous work (*Momoi*, 1967a) by the broken lines.

According to Figs. 12-1 to 12-7 and Figs. 13-1 to 13-7 (the figures relevant to the variation in the windward), it is found that the theory for infinitesimal thickness is capable of explaining the behavior of the wave around the breakwater gap with *thickness ratio* l/d (the term thickness ratio will be used in the following discussion) up to 0.5 in the

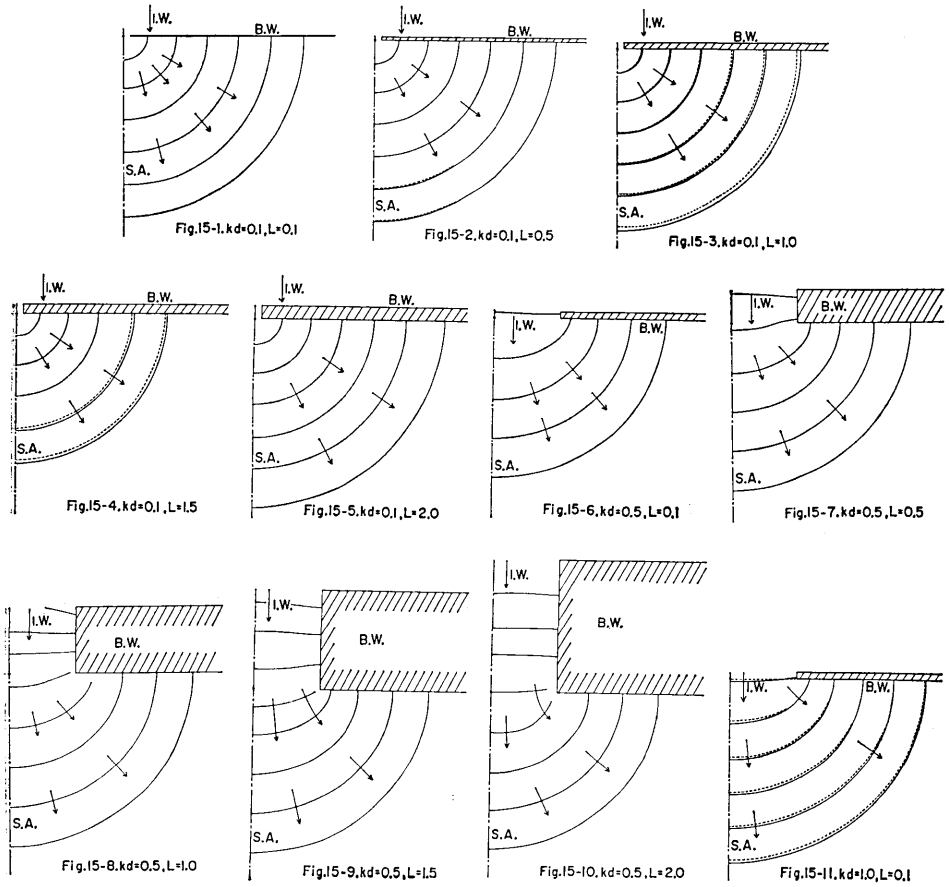

Figs. 15-1 to 15-11. Variation of the phase arg ζ in the leeward waters**.

* The depiction of the figure is made for the conjugate value of ζ obtained in Section 2, which refers to the conversion of the incident wave from $\exp(-i\omega t - iky)$ to $\exp(+i\omega t + iky)$.

** See the footnote of Figs. 10a, b, c and 11a, b, c.

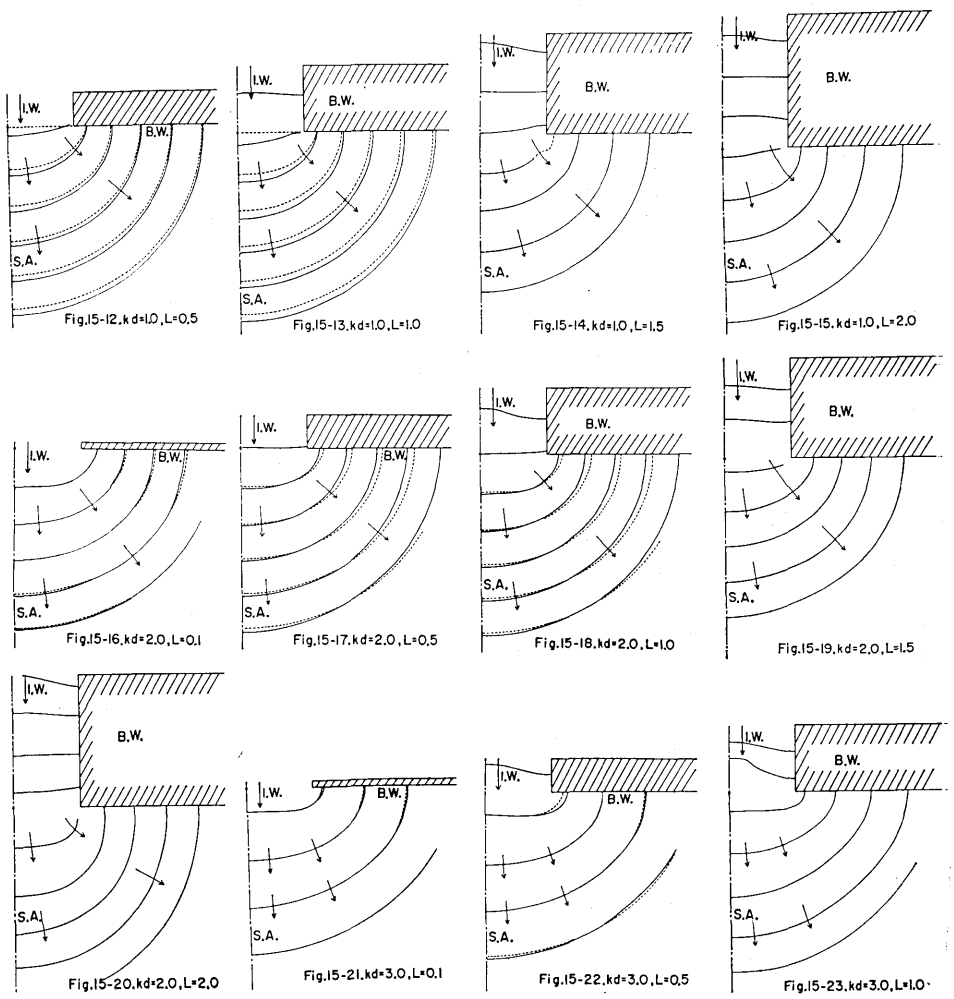

Figs. 15-12 to 15-23. Variation of the phase arg ζ in the leeward waters*.

windward. As for the leeward waters, the agreement of the former and the latter is perceived fairly well for thickness ratio up to 0.1, 0.5, 1.0, 0.5, respectively, for the amplitude variation relating to the parameter $kd=0.1$, 1.0, 2.0, 3.0, (refer to Figs. 14-1 to 14-23) and up to 1.5, 1.0, 1.0, 0.5, for the phase variation (refer to Figs. 15-1 to 15-23). Allowing for the thickness ratio of prevailing breakwaters in harbours and bays, the theory for infinitesimal thickness might be employed in place of the theory for finite thickness to elucidate the behavior of the wave around the breakwater gap in the case of the normal incidence of

* See the footnote of Figs. 10a, b, c and 11a, b, c.

the invading wave.

The figures relevant to the variation of the wave in the gap and the leeward waters (Figs. 14-1 to 14-23 and Figs. 15-1 to 15-23) reveals the following facts. When kd is small (refer to Figs. 14-1 to 14-5 and Figs. 15-1 to 15-5), the contours of the amplitude and phase run in a circular form to suggest strong diffraction. As kd increases from 0.5 to 3.0, the wave transmitted through the gap is directed gradually toward the axis of the gap (refer to Figs. 14-6 to 14-23 and Figs. 15-6 to 15-23). For the case of small thickness ratio (the figures with the parameter $l/d=0.1$), the wave in the gap is about 1.0 in amplitude, increasing in amount with the augmentation of l/d.

4,3. Generated Wave in the Breakwater Gap.

In this section, the wave generated in the breakwater gap is estimated through the following procedure. Let ζ_f and ζ_i be, respectively, the wave heights around the breakwater gap with finite and infinitesimal thickness for the invasion of the incident wave $\exp(+i\omega t+iky)$, which are given by the conjugate expressions of (7) to (11) in Section 2,3 of this paper and (8) to (10) in Section 2,4, of the previous work (*Momoi*, 1967a). The generated wave ζ_{gw} is assessed approximately by the equation

$$\zeta_{gw}\approx\zeta_f-\zeta_i. \tag{50}$$

The illustration of the above equation is given in Fig. 16. The computed range is 0.1 to 4.0 for kd and 0.1 to 2.0 for l/d. The results are presented in Figs. 17-1 to 17-23 for the amplitude and Figs. 18-1 to 18-23 for the phase.

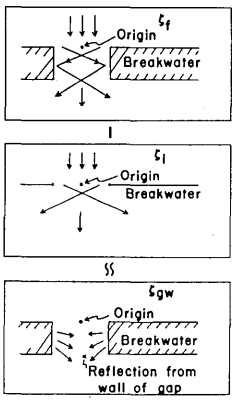

Fig. 16. Illustration of equation (50).

Passing through all the above figures, the wave reflected at the wall of the breakwater gap is found definitely. As would be expected, the above reflected wave is intensified with increasing thickness ratio from 0.1 to 2.0 for each value of kd. The intensification begins to be stronger and stronger as kd increases from 0.5 to 4.0. The portion of the high wave is mainly located along the wall of the gap near the leeward corner, in which the strong reflection of the wave occurs. According to the figures of the phase variation for $kd=3.0-4.0$ and $l/d=1.5-2.0$ (Figs. 18-17, 18-18, 18-22, 18-23), the strong reflection from the nearby part of the leeward corner of the gap is found clearly. As for the high wave in the gap, further study will be made in the later work. Accompanied with the strong reflection in the

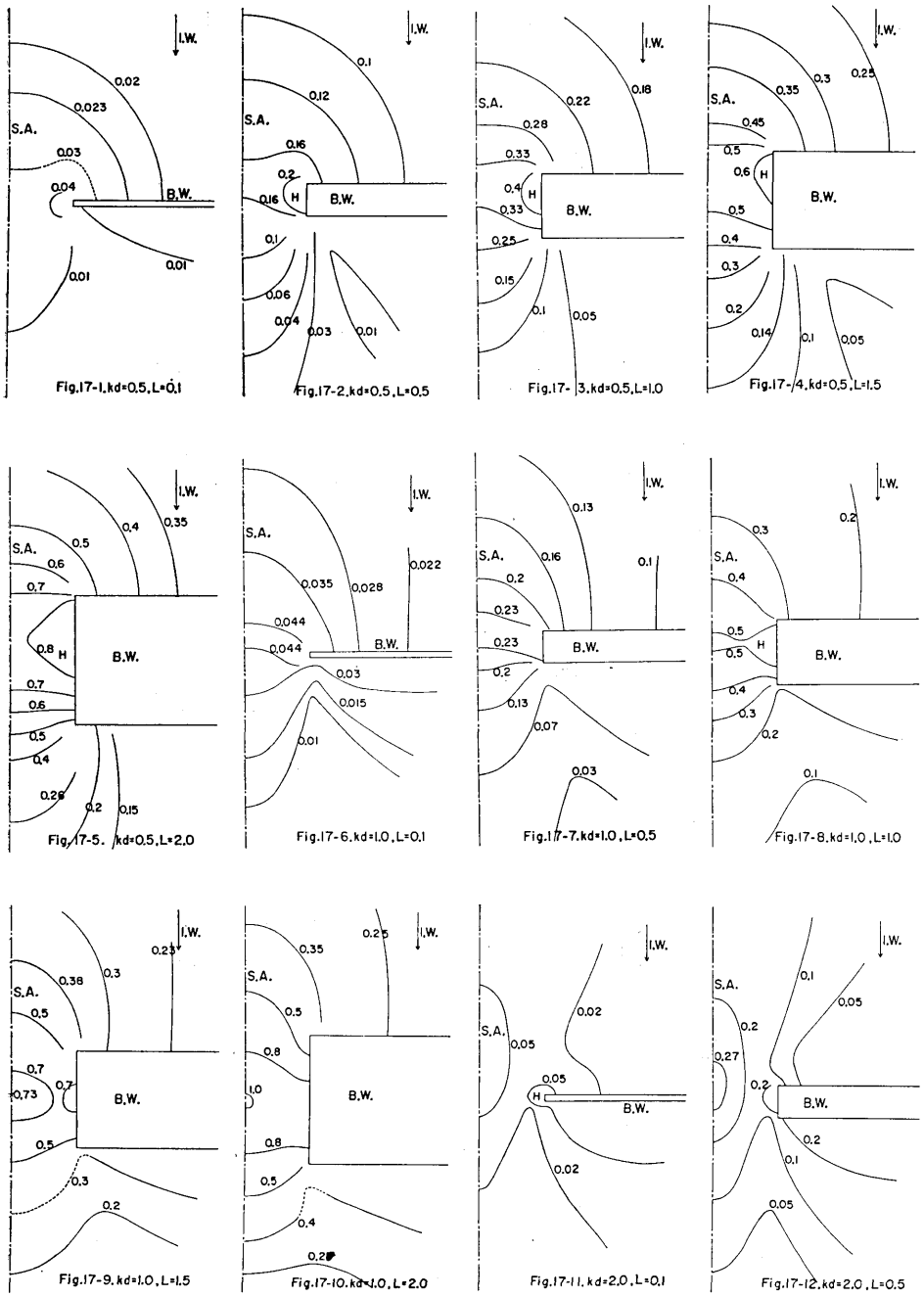

Figs. 17-1 to 17-12. Variation of the amplitude $|\zeta_{gw}|$ of the wave generated in the breakwater gap*.

* See the footnote of Figs. 10a, b, c and 11a, b, c.

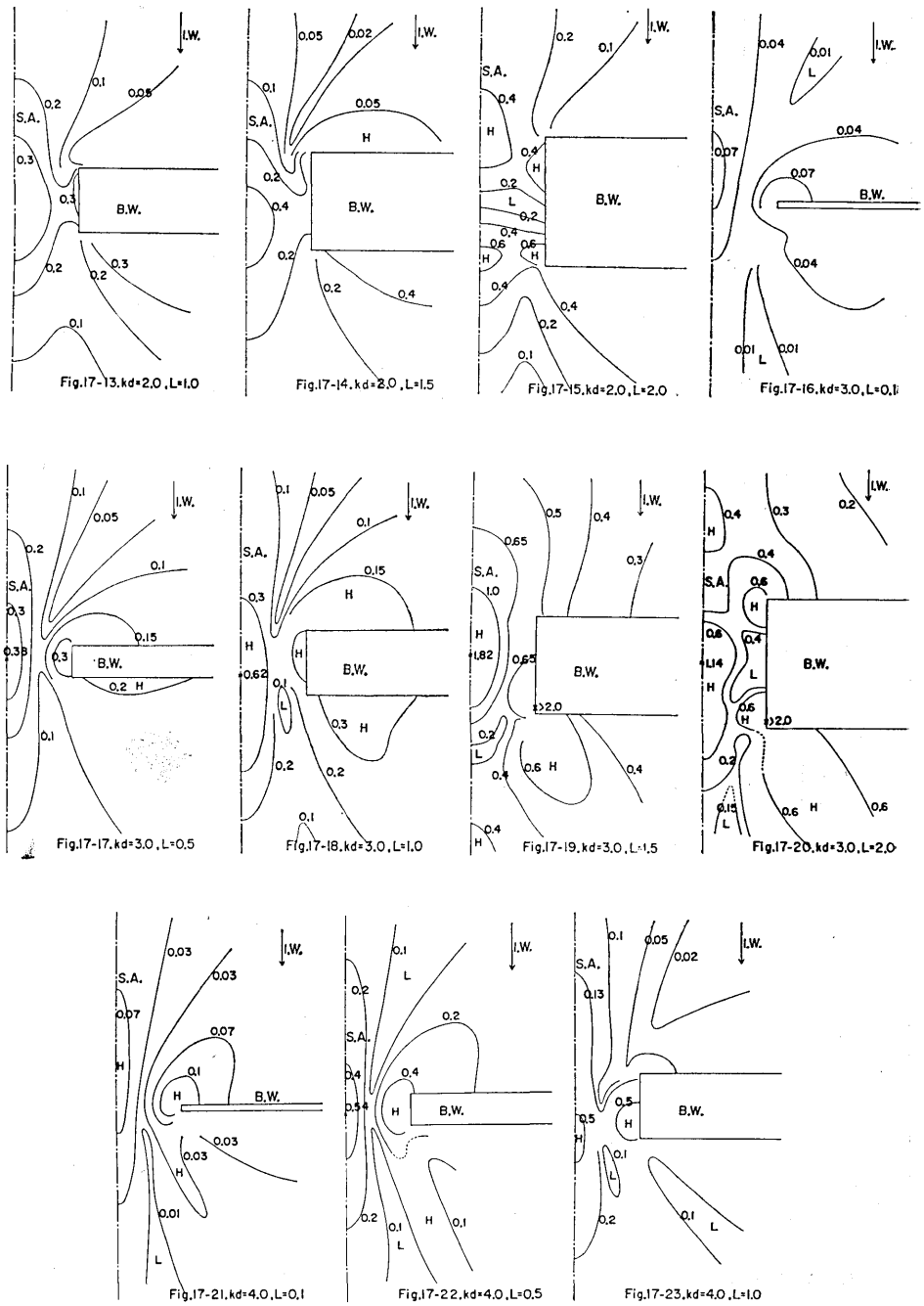

Figs. 17-13 to 17-23. Variation of the amplitude $|\zeta_{gw}|$ of the wave generated in the breakwater gap*.

* See the footnote of Figs. 10a, b, c and 11a, b, c.

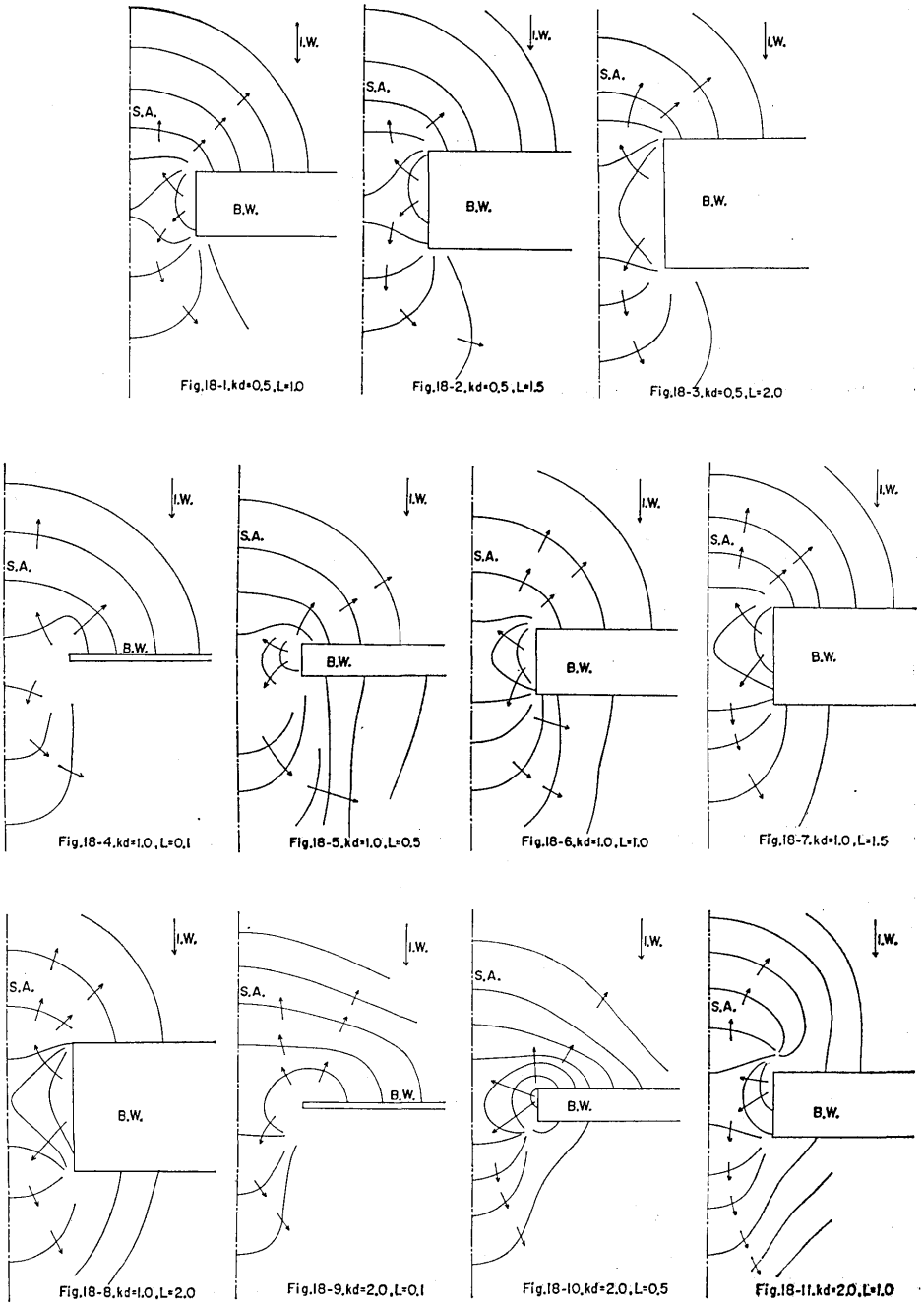

Figs. 18-1 to 18-11. Variation of the phase $\arg \zeta_{gw}$ of the wave generated in the breakwater gap*.

* See the footnote of Figs. 10a, b, c and 11a, b, c.

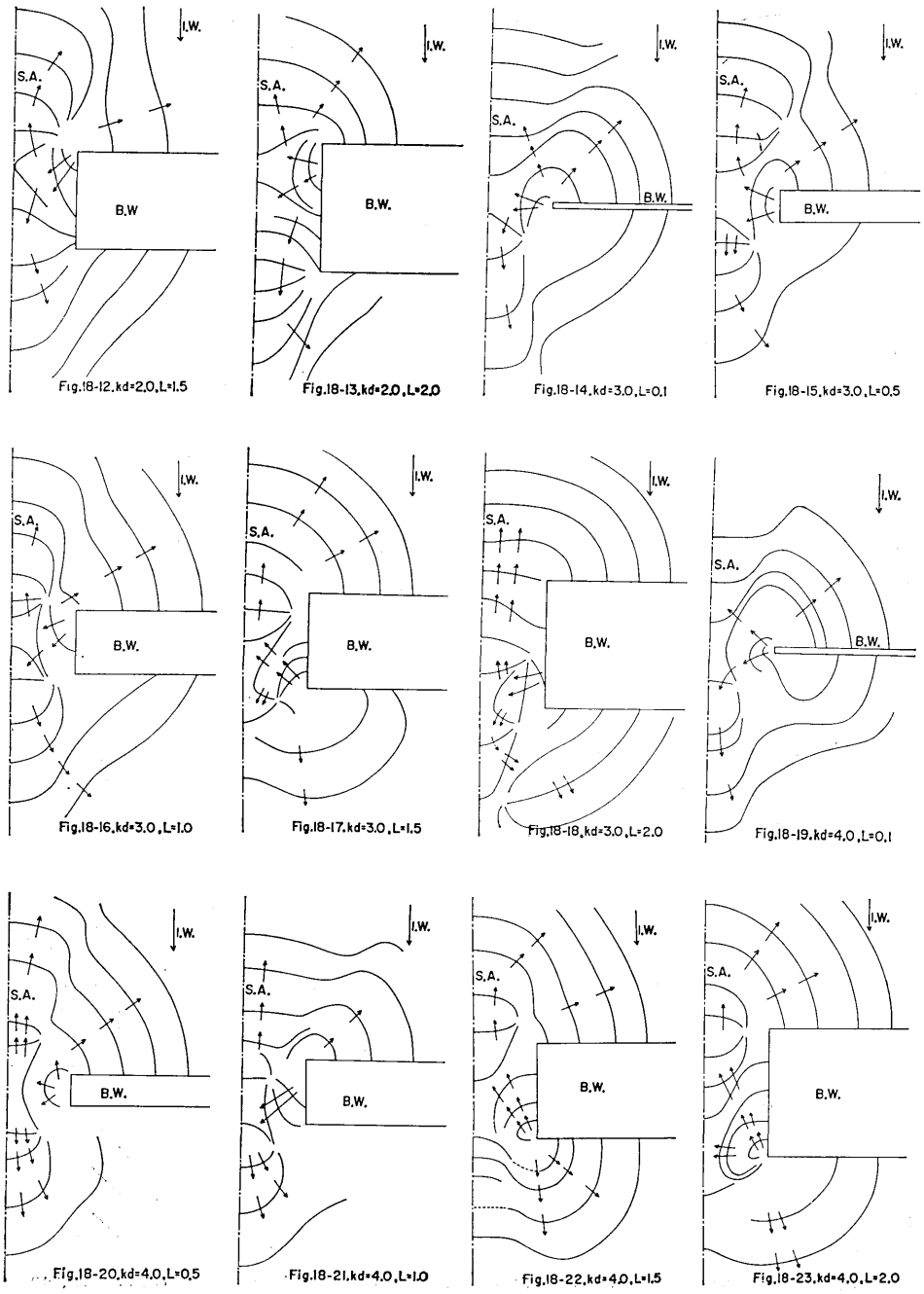

Figs. 18-12 to 18-23. Variation of the phase arg ζ_{gw} in the breakwater gap*.

* See the footnote of Figs. 10a, b, c and 11a, b, c.

gap for the wave of the parameters kd and l/d stated above, a definite scattering of the wave from the leeward corner of the gap toward the leeward waters is found in Figs. 18-17, 18-18, 18-22 and 18-23.

References

MOMOI, T., 1967a, 1967b, 1968a, 1968b, 1968c, 1969a, 1969b, and 1969c, A Long Wave around a Breakwater [I], [II], [III], [IV], [V], [VI], [VII] and [VIII], *Bull. Earthq. Res. Inst.*, **45**, 91-136, **45**, 749-783, **46**, 125-135, **46**, 319-343, **46**, 889-899, **47**, 165-184, **47**, 701-719 and **47**, 875-890.

MOMOI, T., 1968d, A Long Wave in the Vicinity of an Estuary [V], *Bull. Earthq. Res. Inst.*, **46**, 1237-1268.

IPPEN, A. I. and Y. GODA, 1963, Wave induced Oscillations in Harbours, *Hydrodynamics Labo. Rep.* No. 59, MIT.

MITSUI, H., 1966, Distribution of Wave Heights along Harbour and Coastal Structures with Discontinuous Alignments (Part 1), *Proc. 13th CEC, JSCE*, 80-86.

---

33. 有限の厚さをもつ防波堤のまわりの長波 [I]

— 垂直入射の場合 —

地震研究所　桃　井　高　夫

間隙をもった有限の厚さの防波堤に波が垂直に入射したとき，そのまわりにおこる長波が本報告において論じられている．明らかにされた著しい事実として，現実に在在する防波堤のまわりの長波を論ずるのに無限小の厚さの防波堤に対する理論が有効である．